East European Journal of Physics. **1.** 16-25 (2022)
DOI:10.26565/2312-4334-2022-1-03 ISSN 2312-4334

AN INSIGHT INTO THE ELECTRONIC, OPTICAL AND TRANSPORT PROPERTIES OF A HALF HEUSLER ALLOY: NiVSi[†]

Djelti Radouan[a,*], Besbes Anissa[b], Bestani Benaouda[b]
[a]*Technology and Solids Properties Laboratory, Mostaganem University (UMAB) – Algeria*
[b]*SEA2M Laboratory, Mostaganem University (UMAB) – Algeria*
**Corresponding Author: Radouane.djelti@univ-mosta.dz, djeltired@yahoo.fr*
Received November 17, 2021; accepted February 14, 2022

The half-Heusler alloy NiVSi is investigated theoretically by using first-principles calculations based on the density functional theory (DFT). For a better description of the electronic properties, the TB-mBJ potential is used for exchange-correlation potential. The structural, electronic, magnetic, optical and thermoelectric properties was calculated by WIEN2k software. The negative cohesive and formation energies found reveal that the NiVSi is thermodynamically stable. Electronically, the NiVSi is a half-metal with an indirect band gap of 0.73 eV in the spin-down channel whereas the spin up channel is metallic. The total magnetic moment is of 1. Optically, the obtained high absorption coefficient in ultraviolet wavelength range, make the NiVSi useful as effective ultraviolet absorber. Thermoelectrically, a high figure of merit in the p- and n-type region was obtained, what makes this compound very functional for thermoelectric applications. The generation of a fully spin-polarized current make this compound unsuitable for spintronic applications at room temperature, a doping may be a satisfactory solution to improve this property.
Keywords: DFT; mBJ approach; half-metallic; ultraviolet; merit factor.
PACS: 71.20.-b, 72.15.Jf, 72.25.Ba, 73.50.L, 52.70.Kz

The notion of half metallic ferromagnets was established for the first time by de Groot et al. [1]. Since then several researchers paid particular attention to the magnetic half-Heusler (H.H) compounds due to their good physical properties [2-7]. The H.H exhibit fascinating optical and thermoelectric functionalities, those, which present high absorption coefficient and low reflectivity, have become promising candidates for highly efficient solar cells [8-10], while those with high figure of merit (ZT), have gained increasing popularity and are among the new energy resources [11-13]. Numerous studies carried out on H.H compounds have revealed the very good optical, thermoelectric and mechanical performance. The optical investigation conducted by R. Majumder and al., [14] shows that the LuPtBi compound has a good absorption in low energy region and good reflection in vacuum UV region, it exhibit dielectric response even at zero energy. A. Zakutayev [15] synthesized a new half-Heusler compound TaCoSn, which is indicated to possess favorable optical absorption coefficient and high electrical conductivity. According to recent study effected by R. Ahmad and N. Mehmood [16], the NiFeZ, half-Heusler compounds show a half-metallic behaviour with indirect small band gaps and their optical properties are more active at lower energy spectra. Hai-Long Sun et al., [17] have found for the BCaGa, a remarkably high ZT of 7.38 at 700K in the n-type region, while Wendan et al., [18] give a ZT value of 2.43 at 1100 K for the Zr-doped TiPdSn. S.M. Saini [19] shows that the LuNiSb exhibits its best thermoelectric performance at low temperature where the ZT is around 1 at 50K. A. Arunachalam et al [20] give a theoretical analysis of half metallicity and ferromagnetism in NiCrZ (Z = Si, Ge, Ga, Al, In, As), and show that compounds exhibit magnetic interaction and promising figure of merit in magnetic memory element. H.B. Ozisik et al [21] explored the effect of pressure on the electronic properties of half-Heusler NiXSn (X = Zr, Hf) compounds via the GGA approach, they found that both compound are semiconductor with a narrow-band-gap. Beyond a critical pressure of 161 GPa and 229 GPa for NiZrSn and NiHfSn respectively, the compounds become metallic. P. Hermet et al [22] studied the temperature effect on the mechanical properties of NiTiSn half-Heusler. The authors shows that the compound is very useful when a large temperature fluctuations occurs because it remains ductile and robust at 700K and even conserves its very good mechanical properties up to 1500 K. According to this brief bibliographic review, we can conclude that depending to their composition, the Ni based half-Heusler alloys exhibit a wide variety of magnetic, thermoelectric, optical and mechanical properties, which allows them to be believed as very promising half metallic ferromagnetic materials for several technological application. The main objective to this study is to investigate the structural, electronic, optical and thermoelectric behaviour of the NiVSi half-Heusler compound. This research is arranged as follows. Details of computation are given in Section "Computational method". Results and discussion are presented in Section "Results and discussion". A summary of the results is given in Section "Conclusion"

COMPUTATIONAL METHOD

First-principles calculations based on DFT have been conducted to research the structural, electronic, optical and thermoelectric properties of NiVSi half-heusler. Exchange-correlation effects were treated with TB-mBJ potential [23]. The valence electrons for the NiVSi primal cell are $4s^2$ $3d^8$ of Ni, $4s^2$ $3d^3$ of V and $3s^2$ $3p^2$ of Si. The muffin tin radius

[†] ***Cite as***: D. Radouan, B. Anissa, and B. Benaouda, East. Eur. J. Phys. **1**, 16-25 (2022), https://doi.org/10.26565/2312-4334-2022-1-03

(R_{MT}) values of 1.85, 2.1 and 2.5 Bohr were used for Ni, V and Si respectively. Other parameters such as R_{MT} × *wave-vector kmax (*K_{MAX}), k-point mesh and the maximum value of angular momentum (lmax) were selected to 7.0, 16×16×16 and 10 respectively. The optical constants are derived from the complex dielectric function [24-26]. The semi-classical Boltzmann approach [27] as given in the BoltzTraP code was used to investigate the thermoelectric response of NiVSi compound. A fine grid mesh (46×46×46) was used.

RESULTS AND DISCUSSION

Structural properties

The half-Heusler (H.H) is intermetallic compound with general formula XYZ, where X and Y are transition metals and Z a p-block element. The H.H crystallize in the face-centered cubic structure (space group F-43m). The Ni, V and Si atoms are positioned according to one of the three types displayed in Table 1.

Table 1. Wyckoff position of atoms in the unit cell of cubic half-Heusler alloy NiVSi

Type	Ni	V	Si
I	4b (0.5, 0.5, 0.5)	4c (0.25, 0.25, 0.25)	4a (0, 0, 0)
II	4b (0.5, 0.5, 0.5)	4a (0, 0, 0)	4c (0.25, 0.25, 0.25)
III	4c (0.25, 0.25, 0.25)	4b (0.5, 0.5, 0.5)	4a (0, 0, 0)

We have carried out the structural optimization in ferromagnetic (FM) and non-magnetic (NM) configuration for the three possible types of arrangement. From Figure 1 and Table 2, we can see that the ferromagnetic state of the type III arrangement is the most stable among the six possible configurations because it has the lowest energy.

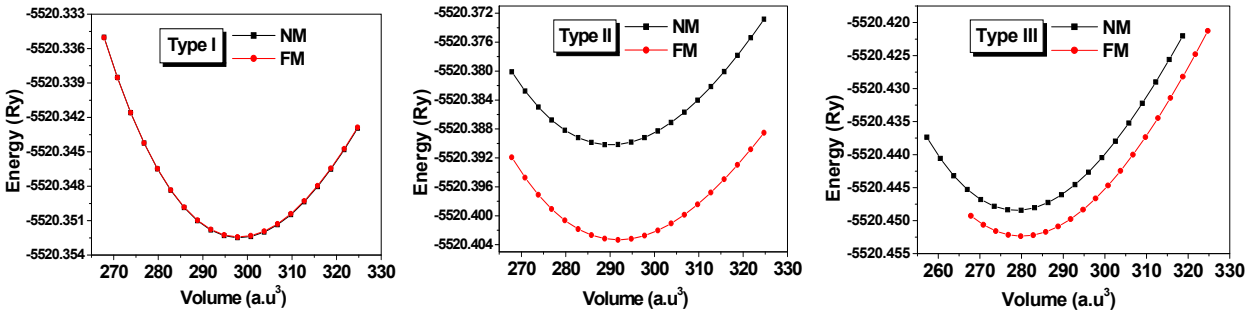

Figure 1. Calculated total energy of NiVSi compound as functions of the unit cell volume for the FM and NM states in each possible atomic arrangement

Table 2. The calculated equilibrium lattice constant a_0, the ground state energies E_0, the bulk modulus B, its pressure derivatives B', the cohesive energy E_C and the formation energy E_f of cubic NiVSi alloy.

Type	State	a_0 (Å)	E_0 (Ry)	B (GPa)	B'	E_C (Ry)	E_f (Ry)
I	FM	5.61	-5520.352411	138.3670	4.15		
	NM	5.61	-5520.352477	138.6531	4.15		
II	FM	5.57	-5520.403317	145.3527	4.97		
	NM	5.56	-5520.390198	152.2824	4.60		
III	**FM**	**5.49** (5.47) [32]	**-5520.452380**	**167.3817**	**4.54**	**--1.417**	**-0.304**(-0.316)[32]
	NM	5.48	-5520.448458	174.6848	4.85		

To ensure the structural stability in the ground state and also to estimate the chemical stability and see a possible synthesis of NiVSi, we have calculated the formation energy (ΔH_f) and cohesive energy (E_{Coh}). The formation enthalpy is defined as [28]:

$$\Delta H_f = E_{NiVSi}^{Total} - \left(E_{Ni}^{bulk} + E_V^{bulk} + E_{Si}^{bulk}\right) \quad (1)$$

Where E_{NiVSi}^{Total}, is the total energy of the NiVSi alloy, $E_{Ni}^{bulk}, E_V^{bulk}$ and E_{Si}^{bulk} are the total energy per atom of Ni, V, and Si in their bulk stable states, respectively. The cohesive energy (E_{Coh}) per formula unit have been calculated using the relation [29]:

$$E_{Coh} = E_{NiVSi}^{Total} - \left(E_{Ni}^{iso} + E_V^{iso} + E_{Si}^{iso}\right) \quad (2)$$

E_{NiVSi}^{Total}, is the total energy of the NiVSi alloy at equilibrium lattice and $E_{Ni}^{iso}, E_V^{iso}, E_{Si}^{iso}$ are the total energies of the isolate atomic components. The negative value of ΔH_f and E_{Coh} (Table 2) confirm the structural and chemical stability of our half-Heusler NiVSi in the type III atomic arrangement with FM state. The crystal structure of NiVSi alloy in the type-III

(FM) given in Figure 2 was plotted by the CrystalMaker 2.7 software [30]. The structure is formed by three interpenetrating fcc sublattices, which are occupied by Ni, V and Si elements.

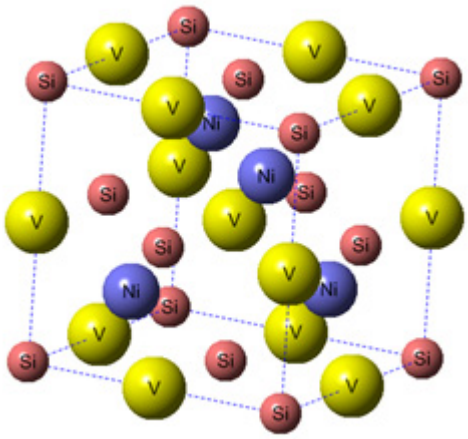

Figure 2. Crystal structure of half-Heusler compound NiVSi

Electronic properties

Fig. 3 shows the spin polarized band structures of the NiVSi half-Heusler alloy. The choice of TB-mBJ approach for this calculation is to obtain an accurate half-metallic gap.

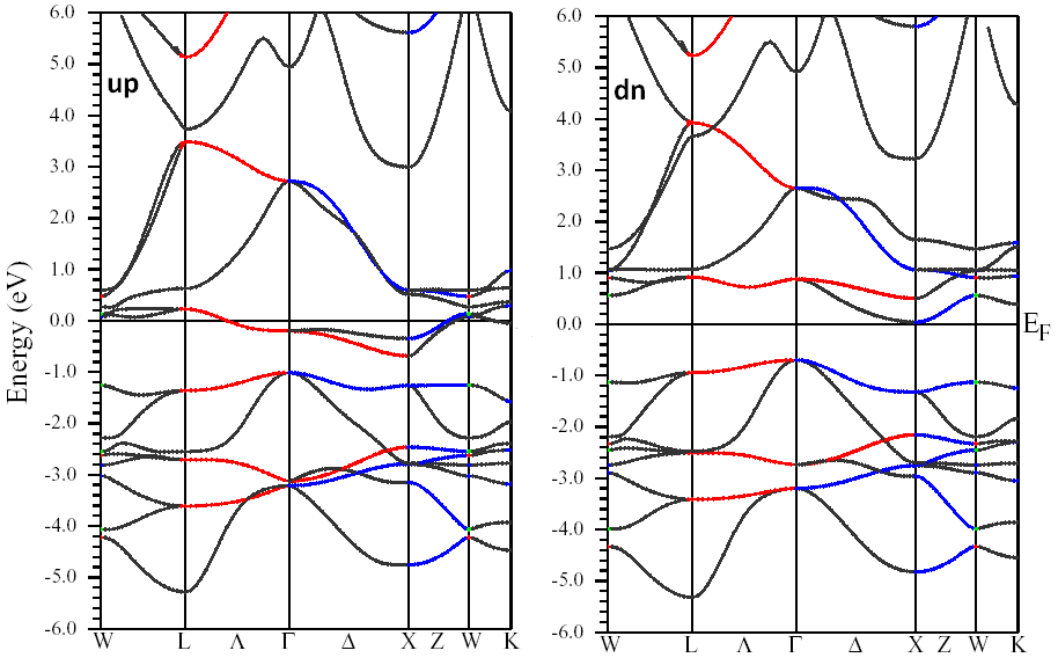

Figure 3. Band structures of NiVSi for both spin channels with mBJ approach

The spin-up (↑) channel, shows a metallic characteristic because the 3d-V band cross the Fermi level. In the spin-down (↓) channel, Fermi level lies inside the forbidden gap, an indirect band gap (between X and Γ points) of about 0.73 eV was observed so confirming the semiconducting nature. This coexistence of metallic nature in spin-up (↑) channel and semiconducting nature in the spin-down (↓) channel leads to the half-metallic nature of NiVSi compound. The origin of the half-metallicity might be due to the strong hybridization between Ni-3d and V-3d states. The calculated band structure presents 100% of spin polarization at the Fermi-level; this can generates a spin-polarized current in the half-metal, only at absolute zero or a temperature very close to zero. According to Fig.3, the Fermi energy is very close to the bottom of conduction band of down spin, that make this compound unsuitable for spintronic applications at room temperature. On the other hand, the 100% of spin polarization at the Fermi-level is very useful to maximizing the efficiency of magneto-electronic devices [31]. In order to study the arrangement of the orbital's in the electronic band structure as well as the electrons involving in the shaping of the band gap, the total and partial density of states (TDOS/PDOSs) of the NiVSi was plotted between -10 and 10 eV Fig. 4(a-b). The dashed line shows the Fermi energy

level (E_F). Fig 4.a, show an asymmetry between spin up (↑) and spin down (↓), this confirms the half-metallic character of NiVSi half-Heusler already predicted by band structure. The energy region around the Fermi level is mainly due to a low contribution of d-Ni states and major contribution of d-V states (Fig 4.b).

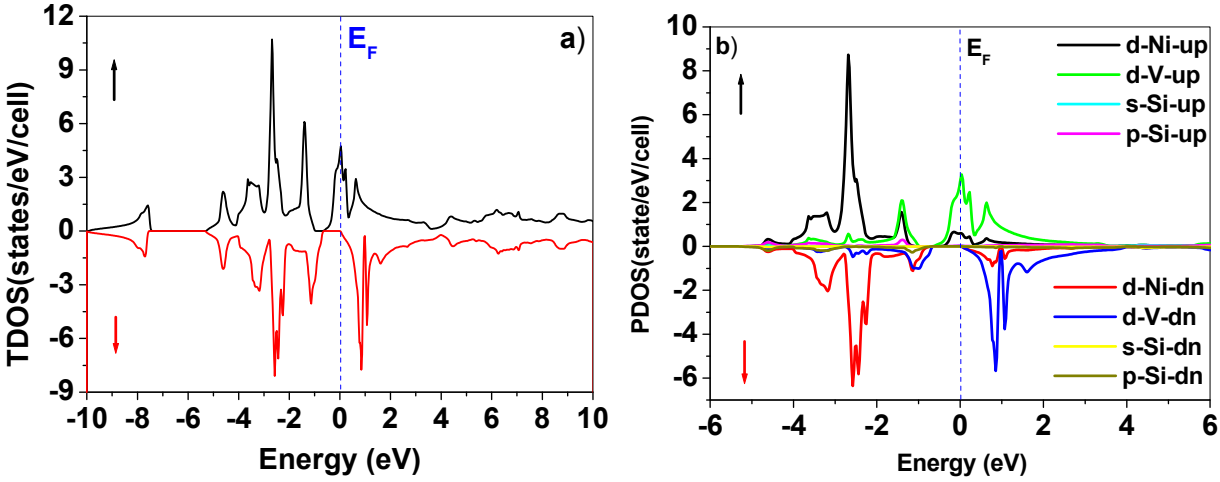

Figure 4. Calculated total and partial density of states with TB-mBJ for NiVSi half-Heusler

We can see that for energies higher than 2eV, the Si-3p state is dominant and for energies lower than -5eV, the principal contribution is due to Si-3s state. In addition, the 3d-V state is most important in the conduction band with a considerable higher DOS values that Ni and Si, whereas in the valence band the 3d-Ni state is the predominant. The combined effect of the crystal field and atoms constituting the alloy induces magnetism. Our study show that the NiVSi half-Heusler possesses FM nature with a total magnetic moment (M_{total}) of 1μB, (Table. 3). The contribution of the interstitial site and partially filled d-states of vanadium generates this total moment. The positive value of the magnetic spin moment is due to vanadium, whereas the low negative value is attributed to silicon. The M_{total} found is slightly higher than obtained by Ma et al [32], this can be justified by the different exchange correlation functional used in the two works.

Table 3. Individual, interstitial and total magnetic moments of NiVSi half-Heusler calculated by GGA and mBJ approximations.

Method	GGA	mBJ	Other work [32]
M_{Ni}	0.0731	0.1138	0.097
M_V	0.8890	0.8981	0.841
M_{Si}	-0.0349	-0.0406	-0.040
$M_{interstitiels}$	0.0738	0.0286	
M_{total}	1.0011	1.0000	0.9582

Optical properties

The optoelectronic applications of a material require in-depth knowledge of their optical properties. In order to describe the interaction of photons with NiVSi alloy, the calculation of optical properties such as polarization, absorption, reflectivity, refractive index and loss energy is necessary. All the optical properties cited above derive from the complex dielectric function $\boldsymbol{\varepsilon(\omega)}$ $(\boldsymbol{eq.3})$.

$$\boldsymbol{\varepsilon(\omega) = \varepsilon_1(\omega) + i\varepsilon_2(\omega)} \tag{3}$$

Where $\boldsymbol{\varepsilon_2(\omega)}$ represents the real transition between the occupied and unoccupied states while $\boldsymbol{\varepsilon_1(\omega)}$ depicts the electronic polarizability under incident light [33]. The imaginary part of the dielectric function $\boldsymbol{\varepsilon_2(\omega)}$ is derived from the electronic band structure computations with the help of the following relation

$$\boldsymbol{\varepsilon_2(\omega) = \left(\frac{4\pi^2 e^2}{m^2\omega^2}\right)\sum_{i,j}\int\langle i|M|j\rangle^2 f_i(1-f_i)\delta(E_j - E_i - \omega)d^3k} \tag{4}$$

Where $\boldsymbol{e, m, \omega}$ and $\boldsymbol{M}$ represent the electron charge, electron mass, photon frequency and dipole matrix, respectively. $\boldsymbol{E_i}$ is the electron energy of the initial state, $\boldsymbol{E_j}$ is the electron energy of the final state, and $\boldsymbol{f_i}$ is the Fermi occupation factor of the single-particle state $\boldsymbol{i}$. The real part $\boldsymbol{\varepsilon_1(\omega)}$ of the dielectric function derives from $\boldsymbol{\varepsilon_2(\omega)}$ by using the Kramers Kronig relations [34-36]:

$$\varepsilon_1(\omega) = 1 + \frac{2}{\pi} P \int_0^{\infty} \frac{\omega' \varepsilon_2(\omega')}{\omega'^2 - \omega^2} d\omega' \quad (5)$$

Where P is the Cauchy principal value.

Other optical parameters like the absorption coefficient $a(\omega)$, reflectivity $R(\omega)$ and refractive index $n(\omega)$ can be obtained from the calculated values of the real and imaginary parts of the dielectric function [37]:

$$a(\omega) = \frac{\sqrt{2\omega}}{c}\left(\sqrt{\varepsilon_1^2(\omega) + \varepsilon_2^2(\omega)} - \varepsilon_1(\omega)\right)^{1/2} \quad (6)$$

$$R(\omega) = \left|\frac{\sqrt{\varepsilon(\omega)} - 1}{\sqrt{\varepsilon(\omega)} + 1}\right|^2 \quad (7)$$

$$n(\omega) = \left[\frac{\sqrt{\varepsilon_1{}^2(\omega) + \varepsilon_2{}^2(\omega)} + \varepsilon_1(\omega)}{2}\right]^{1/2} \quad (8)$$

As the lattice parameters are constant (cubic structure), the obtained optical properties are isotropic (same dielectric tensor). The variations versus energy of real part $\varepsilon_1(\omega)$ and imaginary part $\varepsilon_2(\omega)$ of dielectric function (ω) are plotted in Fig. 5a.

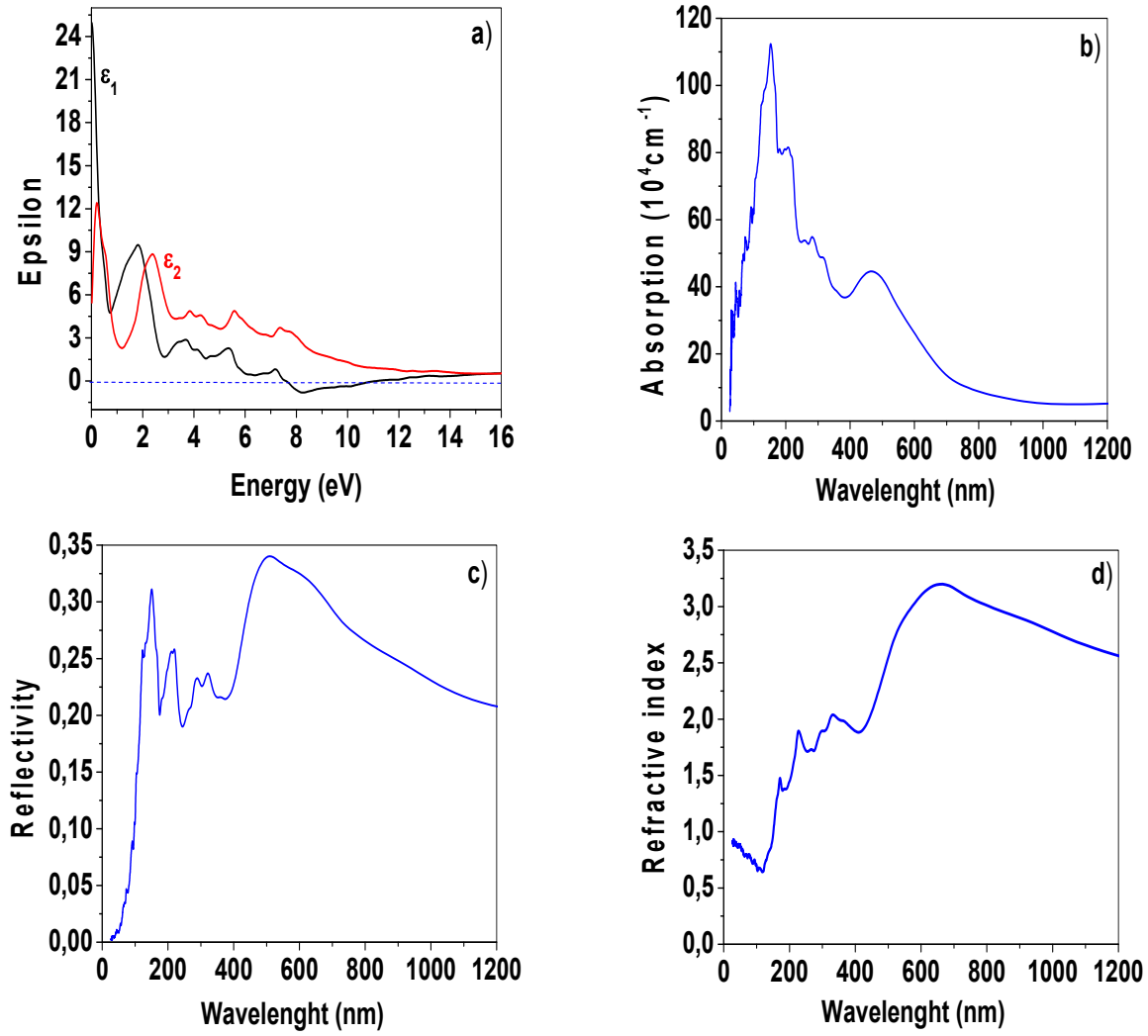

Figure 5. (a) Dielectric function, (b) absorption coefficient**,** (c) reflectivity and (d) refractive index**)** for NiVSi compound by using mBJ approximation.

The light absorption by the material is described by the imaginary part of the dielectric function $\varepsilon_2(\omega)$, this is *associated* to the absorption of the incident energy due to the different electronic transitions caused by the impact energies greater than the band-gap. $\varepsilon_2(\omega)$ starts at 0eV and attain its maximum value of 12.35 in the infrared domain; domain

characterized by minimal dispersion of light due to the low energy. We can see also that $\boldsymbol{\varepsilon_2(\omega)}$ show six absorption peaks located at 0.28 eV, 2.35 eV, 4.03 eV, 4.31 eV, 5.59 eV and 7.39 eV. According to the total and partial density of states (TDOS/PDOS) (Fig 4), these peaks can be related to the inter-band transitions between Si-3p, Ni-3d and V-3d states. The real part of dielectric function $\boldsymbol{\varepsilon_1(\omega)}$ depicts the electronic polarizability under an incident light, its static value at zero photon energy $\boldsymbol{\varepsilon_1(0)}$ is inversely proportional to the band gap (Eg) (Penn model) [38].

$$\boldsymbol{\varepsilon_1(0) = 1 + \left(\frac{h.\omega_P}{E_g}\right)^2} \tag{9}$$

Where $\boldsymbol{\omega_P}$ is the plasma frequency.

The obtained value of $\boldsymbol{\varepsilon_1(0)}$ is 25.08. In the energy range from zero to 7.72 eV, $\boldsymbol{\varepsilon_1(\omega)}$ show positive values, which means the photons, propagate through the material, whereas in the UV range from 7.72 to 10.48 eV, $\boldsymbol{\varepsilon_1(\omega)}$ takes negative values, the compound reflects completely the incident radiation and exhibits a metallic character in this region. Beyond 10.48 eV, the values of real part $\boldsymbol{\varepsilon_1(\omega)}$ fluctuate around 0. The optical absorption measures the strength of the interaction between light and material, its knowledge is essential for any development of opto-electronic device. The absorption coefficient was calculated versus radiation wavelengths in the UV-Visible-IR range. From Fig.5b we can see that the NiVSi display high level of interband absorption, the presence of the low energy gap in spin-down band structure spectrum, match with the principal peak obtained at wavelength of 154 nm (ultraviolet range). We note that the increase of photons energy leads to a proportional diminution in the wavelength. The absorption is very small at low energy (Infrared range) then increases to reach its maximum of 1171139 cm^{-1} in the UV region; this means that the photons, which excite electrons of the conduction band, was absorbed. We can remark also that the absorption coefficient is not constant for photon energies greater than the gap, but depends, heavily on wavelength. The reflectivity R(ω) which describes the ratio between the reflected energy to total incident energy is plotted versus wavelength in Fig. 5c. The compound present two major peaks, located below 152 nm (UV range) and above 506 nm (visible region). The utmost values of reflectivity is mostly due to the resonance Plasmon [39]. The minimum value of R(ω), is observed in UV range at 241 nm, whereas in all the UV-visible domain, the value of reflectivity is less than 35%. The decrease in reflectivity noted from 510 nm implies that a substantial amount of photon energy is transmitted through the material. It is to note that the static value of reflectivity R (0) is about 44%. The interaction of electromagnetic radiation with a non-uniform medium such as material causes a change in the path of the radiation by refraction. From Fig 5d, we can see that the index refraction $n(\omega)$ reaches its maximum value of 3.22 at 661 nm, and then gradually decreases. This can be explained by the fact that the NiVSi alloy absorbs high-energy photons and can no longer act as a transparent matter [40]. The static refractive index $n(0)$ is 5.01, according to equation $n^2(0) = \varepsilon_1(\omega)$, we can deduct the static dielectric constant $\varepsilon_1(0)$ is about 25.11, which is fundamentally according with the result of Fig. 5(a). The refractive index remain positive in the considered range of energy, this is due to the linearity of NiVSi to the frequency of light [41]. Finally, as suggestion for future researches, the bandgap of NiVSi half-Heusler can be modulated or improved by selective doping to have a strong optical absorption, which will allow subsequently to involve this material in several optoelectronic devices such as photovoltaic cells.

Thermoelectric properties

The present thermoelectric study is motivated by the narrow band gap of NiVSi, property that allows a good diffusion of the phonons and which reduces in parallel the thermal conductivity of the network. The transport properties are going to be computed with BoltzTraP code (under a constant relaxation time approximation of the charge carriers) [27], where the electrical conductivity $\boldsymbol{(\sigma/\tau)}$, thermal conductivity $\boldsymbol{(\kappa/\tau)}$, Seebeck coefficient (S) and Merit factor (ZT) will be investigated as function of chemical potential (μ) in range between – 0.15 to 0.15 eV. Semi-classical Boltzmann transport equations are used to calculate the number of thermoelectric coefficients, which can be represented as follows [42-43]:

$$\boldsymbol{\sigma_{\alpha\beta}(T,\mu) = \frac{1}{\Omega}\int \sigma_{\alpha\beta}(\varepsilon)\left[-\partial f_\mu(T,\varepsilon)\right]d\varepsilon} \tag{10}$$

$$\boldsymbol{\kappa_{\alpha\beta}(T,\mu) = \frac{1}{e^2 T\Omega}\int \sigma_{\alpha\beta}\varepsilon(\varepsilon-\mu)^2 \ \frac{\partial f_\mu(T,\varepsilon)}{d\varepsilon}} \tag{11}$$

$$\boldsymbol{S = \frac{e}{T\sigma}\int \sigma_{\alpha\beta}(\varepsilon)(\varepsilon-\mu)\left[\frac{-\partial f_\mu(T,\varepsilon)}{\partial\varepsilon}\right]} \tag{12}$$

$$\boldsymbol{ZT = \frac{S^2\sigma T}{\kappa}} \tag{13}$$

Where $\boldsymbol{\Omega, f, \mu, \sigma, \kappa, S}$ and $\boldsymbol{Z}$ represents the unit-cell volume, Fermi-Dirac distribution function, chemical potential, electrical conductivity, thermal conductivity, Seebeck coefficient and merit factor respectively. The variation of electrical

conductivity **(σ/τ)** which depicts the fluency at which electrical charge can flow in matter is show in Fig 6.a. The starting points of **(σ/τ)** for p-type (μ < 0) and n-type (μ > 0) regions are situated at chemical potentials of -0.05 μ(eV) and 0.01 μ(eV) respectively. Between these points, **(σ/τ)** is zero; while a clear, improvement observed beyond these values. A value peak of $2.94.10^{20}$ $(\Omega m)^{-1}$ is observed in p-type at 0.122 μ(eV), while the n-type show a value peak of 7.510^{20} $(\Omega m)^{-1}$ at 0.15 μ(eV). The **(σ/τ)** values are not influenced by changing the levels of temperature (300, 600 and 900K). The capacity of the half-heusler NiVSi to transfer heat is studied in this section through the calculation of its thermal conductivity **(κ/τ)**. As show in Fig.6b, the profile of thermal conductivity **(κ/τ)** curves is the same to the electrical conductivity **(σ/τ)**, except that here the temperature change has a significant influence on the **(κ/τ)** values. At 300 K, the thermal conductivity **(κ/τ)** is weak then it sudden increases with the increasing in temperature especially in the n-type region, this is due to electron-phonon scattering [44]. Fig 6.c gives the Seebeck coefficient (S) which demonstrates the capacity to generate electric potential from the temperature gradient. The principal peak of Seebeck coefficient occur between -0.052 and 0.007 eV, outside this range, the curve tends rapidly to zero. At 300 K, the magnitude of Seebeck coefficient is about 1235 μV/K (-0.026eV), this value is reached in the p-type region. For temperature higher than 300 K, the Seebeck coefficient diminish due to the increase in the holes and in thermal energy [45]. The NiVSi compound is a promising thermoelectric material, exhibiting a high Seebeck coefficient due to its half-metallic character and its narrow band-gap. The scale of the thermoelectric efficiency is measured by the figure of merit (ZT). A high ZT value requires a high electrical conductivity and Seebeck coefficient and low thermal conductivity [46]. The ZT curves obtained at different temperature exhibit a global similarity: the peaks are located at almost similar energies and their magnitudes decrease with increasing in temperature (Fig 6.d).

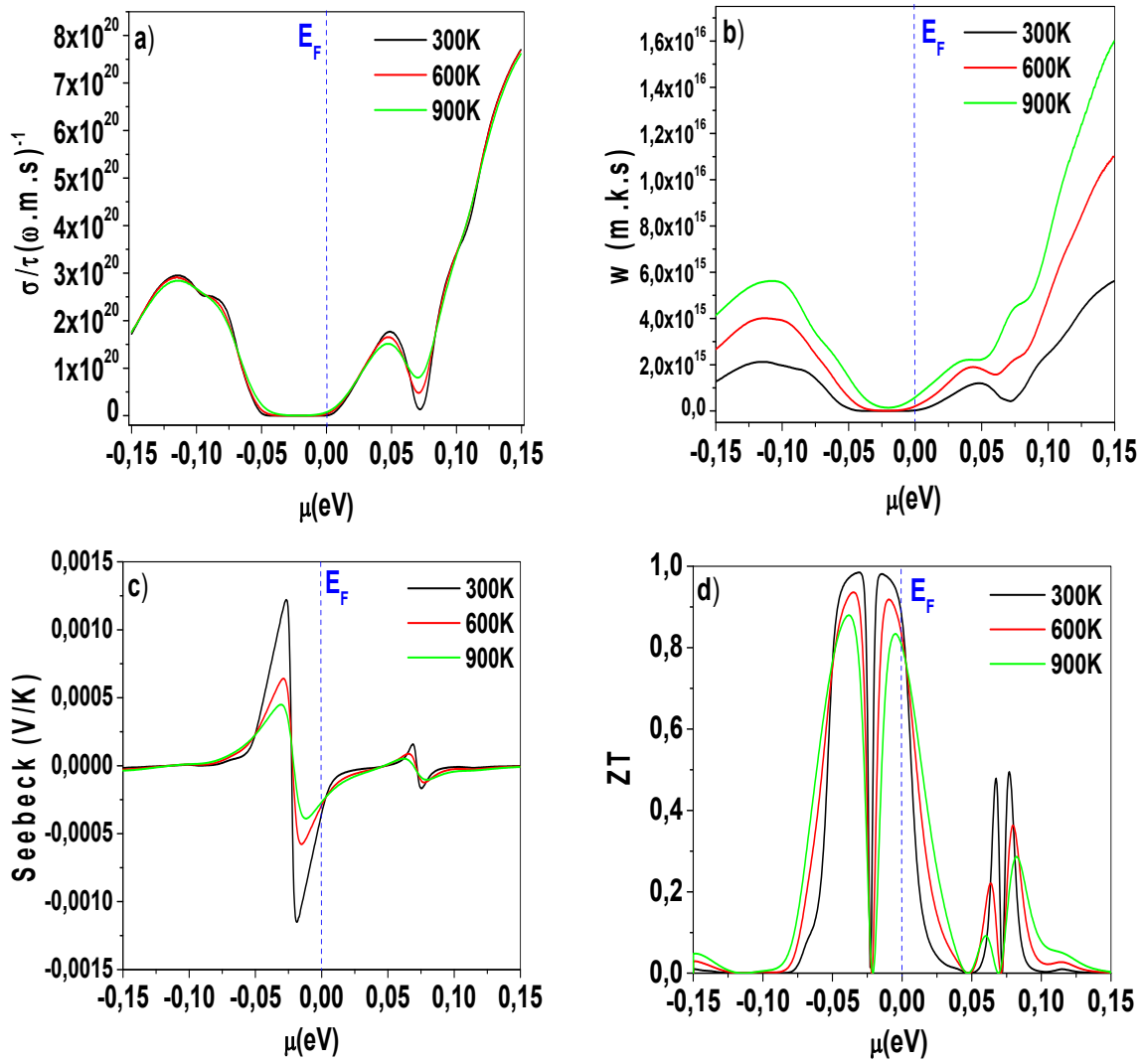

Figure 6. Evolution of (a) electrical conductivity, (b) thermal conductivity, (c) Seebeck coefficient, and (d) Merit factor (ZT) versus chemical potential at different temperatures.

At the chemical potential corresponding to the Fermi level (dashed line) the computations gives a ZT values not less than 0.83 for all considered temperature. Around the zero chemical potential, the conduction charges are small from where a minimum electronic thermal conductivity, which made it possible to have these high merit factors. The maximal ZT

value is 0.98 (300 K), 0.93 (600 K) and 0.87 (900 K) for p-type doping, and it is 0.49 (300 K), 0.36 (600 K) and 0.29 (900 K) for n-type doping. The values of the merit factor is higher for the negative chemical potential compared to the positive one, and the width of the peak in the $\mu < 0$ region is larger than that in the $\mu > 0$ region. The NiVSi tends to be a p-type semiconductor, because the holes rather than the doping of electrons gives the best thermoelectric performance.

The obtained values of ZT are larger to those reported for many half-Heusler compounds such as PdZrGe [47], ZrFeSi [48], RbBaB [49], XLiSn [50], RhTiSb [51].

CONCLUSION

We performed first principles calculations of the structural, electronic, optical and thermoelectrics properties of NiVSi half-Heusler compound using FP-LAPW formalism and semi-classical Boltzmann transport theory. The electronic investigation discloses that the NiVSi is half-metallic with indirect band gap nature, this half-metallicity suggest potential applications in spintronic devices. The magnetic study reveals that NiVSi is a weak ferromagnetic material with 100% spin polarization at Fermi level, this can produces a spin-polarized current useful to maximizing the efficiency of magneto-electronic devices. The optical properties computations attest that the NiVSi has a broad absorption band in the ultraviolet region, its high absorption coefficient of 112.10^4 cm^{-1} suggest that it can be used as ultraviolet absorber. In addition, the compound is transparent in the considered infrared range [780-1200 nm]. Thermoelectric computations disclose that the holes are the main charge carriers. At a room temperature, the obtained merit factor is about 0.98, thus affirming that the NiVSi is a promising material for applications in the thermoelectric domain. Finally, we suggest that to boost the spintronic performance of this alloy, a doping remain necessary to move the bottom of the conduction band away from the Fermi level.

ORCID IDs

Djelti Radouan, https://orcid.org/0000-0002-0762-5818; **Bestani Benaouda**, https://orcid.org/0000-0002-1104-0900

REFERENCES

[1] R. De Groot, F. Mueller, P. Van Engen, and K. Buschow, New class of materials: half-metallic ferromagnets, Phys. Rev. Lett. **50**(25), 2024 (1983). https://doi.org/10.1103/PhysRevLett.50.2024

[2] M. Zhang, X. Dai, H. Hu, G. Liu, Y. Cui, Z. Liu, J. Chen, J. Wang, and G. Wu, Search for new half-metallic ferromagnets in semi-Heusler alloys NiCrM (M = P, As, Sb, S, Se and Te), J. Phys.: Condens. Matter. **15**, 7891 (2003). https://doi.org/10.1088/0953-8984/15/46/008

[3] H. Luo, Z. Zhu, G. Liu, S. Xu, G. Wu, H. Liu, J. Qu, and Y. Li, Ab-initio investigation of electronic properties and magnetism of half-Heusler alloys XCrAl (X = Fe, Co, Ni) and NiCrZ (Z = Al, Ga, In), Physica B, **403**, 200 (2008). https://doi.org/10.1016/j.physb.2007.08.214

[4] S.H. Wang, H.M. Cheng, R.J. Wu, and W.H. Chao, Structural and thermoelectric properties of HfNiSn half-Heusler thin films, Thin Solid Films, **518**(21), 5901 (2010). https://doi.org/10.1016/j.tsf.2010.05.080

[5] L. Huang, R. He, S. Chen, H. Zhang, K. Dahal, H. Zhou, H. Wang, Q. Zhang, and Z. Ren, A new n-type half-Heusler thermoelectric material NbCoSb, Materials Research Bulletin, **70**, 773 (2015). https://doi.org/10.1016/j.materresbull.2015.06.022

[6] S.V. Pedersen, J.R. Croteau, N. Kempf, Y. Zhang, D.P. Butt, and B.J. Jaques, Novel synthesis and processing effects on the figure of merit for NbCoSn, NbFeSb, and ZrNiSn based half-Heusler thermoelectrics, Journal of Solid State Chemistry, **285**, 121203 (2020). https://doi.org/10.1016/j.jssc.2020.121203

[7] A. Saini, S. Nag, R. Singh, and R. Kumar, Enhacement in the thermoelectric performance of half-Heusler alloy LiScGe under hydrostatic pressure, Journal of Alloys and Compounds, **818**, 152929 (2020). http://dx.doi.org/10.1016/j.jallcom.2019.152929

[8] S. Kacimi, H. Mehnane, and A. Zaoui, I–II–V and I–III–IV half-Heusler compounds for optoelectronic applications: Comparative ab initio study, Journal of Alloys and Compounds, **587**, 451 (2014). https://doi.org/10.1016/j.jallcom.2013.10.046

[9] F. Parvin, M.A. Hossain, I. Ahmed, K. Akter, and A.K.M.A. Islam, First-principles calculations to investigate mechanical, optoelectronic and thermoelectric properties of half-Heusler p-type semiconductor BaAgP, Results in Physics, **23**, 104068 (2021). https://doi.org/10.1016/j.rinp.2021.104068

[10] D. Kieven, R. Klenk, S. Naghavi, C. Felser, and T. Gruhn, I-II-V half-Heusler compounds for optoelectronics: Ab initio calculations, Phys. Rev. B, **81**, 075208 (2010). https://doi.org/10.1103/PhysRevB.81.075208

[11] T. Sekimoto, K. Kurosaki, H. Muta, and S. Yamanaka, Thermoelectric Properties of (Ti, Zr, Hf) CoSb Type Half-Heusler Compounds, Materials Transactions, **46**, 1481 (2005). https://doi.org/10.2320/matertrans.46.1481

[12] A. Page, P.F.P. Poudeu, and C. Uher, A first-principles approach to half-Heusler thermoelectrics: Accelerated prediction and understanding of material properties, Journal of Materiomics, **2**, 104 (2016). https://doi.org/10.1016/j.jmat.2016.04.006

[13] K. Xia, C. Hu, C. Fu, X. Zhao, and T. Zhu, Half-Heusler thermoelectric materials, Appl. Phys. Lett. **118**, 140503 (2021). https://doi.org/10.1063/5.0043552

[14] R. Majumder, and Md.M. Hossain, First-principles study of structural, electronic, elastic, thermodynamic and optical properties of topological superconductor LuPtBi. Comput. Condens. Matter, 21, (2019) e00402. https://doi.org/10.1016/j.cocom.2019.e00402

[15] A. Zakutayev, X. Zhang, Theoretical Prediction and Experimental Realization of New Stable Inorganic Materials Using the Inverse Design Approach, J. Am. Chem. Soc. **135**(27), 10048 (2013). https://doi.org/10.1021/ja311599g

[16] R. Ahmad, and N. Mehmood, Theoretical investigations of properties of new half-Heusler compounds NiFeZ (Z = Si, Ge), J. Supercond. Nov. Magn. **31**(19), 1751 (2018). https://doi.org/10.1007/s10948-017-4378-9

[17] Hai-Long Sun, Chuan-Lu Yang, Mei-Shan Wang, and Xiao-Guang Ma, Remarkably High Thermoelectric Efficiencies of the Half-Heusler Compounds BXGa (X = Be, Mg, and Ca), ACS Appl. Mater. Interfaces, **12**, 5838 (2020). https://doi.org/10.1021/acsami.9b19198
[18] Z. Wendan, L. Yong, L. Yunsheng, W. Jiahua, H. Zhiling, and S. Xiaohong, Structural and thermoelectric properties of Zr-doped TiPdSn half-Heusler compound by first-principles calculations. Chem. Phys. Lett. **741**, 137055 (2000). https://doi.org/10.1016/j.cplett.2019.137055
[19] S.M. Saini, Structural, electronic and thermoelectric performance of narrow gap LuNiSb half Heusler compound: Potential thermoelectric material, Physica B, **610**, 412823 (2021). https://doi.org/10.1016/j.physb.2021.412823
[20] A.Arunachalam, R. Rajeswarapalanichamy, and K. Iyakutti, Half metallic ferromagnetism in Ni based half Heusler alloys, Computational Materials Science, **148**, 87 (2018). https://doi.org/10.1016/j.commatsci.2018.02.026
[21] H B Ozisik et al., Ab-initio calculations on half-Heusler NiXSn (X =Zr, Hf) compounds: electronic and optical properties under pressure, Indian J. Phys. **91**(7), 773 (2017). https://doi.org/10.1007/s12648-017-0971-9
[22] P. Hermet et al., Thermal dependence of the mechanical properties of NiTiSn using first-principles calculations and high-pressure X-ray diffraction, Journal of Alloys and Compounds, **823**, 153611 (2020). https://doi.org/10.1016/j.jallcom.2019.153611
[23] F. Tran, and P. Blaha, Accurate Band Gaps of Semiconductors and Insulators with a Semi local Exchange-Correlation potential, Phys. Rev. Lett. **102**, 226401 (2009). https://doi.org/10.1103/PhysRevLett.102.226401
[24] S. Adachi, Properties of Semiconductor Alloys: Group-IV, III-V and II-VI Semiconductors (John Wiley & Sons, 2009). DOI:10.1002/9780470744383
[25] J.Sun, H.T.Wang and N.B.Ming, Optical properties of heterodiamond B_2CN using first-principles calculations, Appl. Phys. Lett. **84**, 4544 (2004). https://doi.org/10.1063/1.1758781
[26] J.M. Hu, S.P. Huang, Z. Xie, H. Hu, and W.D. Cheng, First-principles study of the elastic and optical properties of the pseudocubic Si_3As_4, Ge_3As_4 and Sn_3As_4, J. Phys.: Condens. Matter, **19**, 496215 (2007). https://doi.org/10.1088/0953-8984/19/49/496215
[27] G.K.H. Madsen, D.J. Singh, and BoltzTraP. A code for calculating band-structure dependent quantities, Comput. Phys. Commun. **175**, 67 (2006). https://doi.org/10.1016/j.cpc.2006.03.007
[28] E. Zhao, and Z. Wu, Electronic and mechanical properties of 5d transition metal mononitrides via first principles, J. Solid State Chem. **181**, 2814 (2008). https://doi.org/10.1016/j.jssc.2008.07.022
[29] J.S. Zhao, Q. Gao, L. Li, H.H. Xie, X.R. Hu, C.L. Xu, and J.B. Deng, First-principles study of the structure, electronic, magnetic and elastic properties of half-Heusler compounds LiXGe (X = Ca, Sr and Ba), Intermetallics, **89** 65 (2017). https://doi.org/10.1016/j.intermet.2017.04.011
[30] Crystalmaker software, http://www.crystalmaker.com
[31] N. Mehmood, R. Ahmad, and G. Murtaza, Ab initio investigations of structural, elastic, mechanical, electronic, magnetic, and optical properties of half-Heusler compounds RhCrZ (Z = Si, Ge), J. Supercond. Nov. Magn. **30**, 2481 (2017). https://doi.org/10.1007/S10948-017-4051-3
[32] J. Ma et al., Computational investigation of half-Heusler compounds for spintronic applications, Phys. Rev. B, **95**, 024411 (2017).
[33] B. Amin, I. Ahmad, M. Maqbool, S. Goumri-Said, and R. Ahmad, Ab initio study of the bandgap engineering of $Al_{1-x}Ga_xN$ for optoelectronic applications, J. Appl. Phys. **109**, 023109 (2011). https://doi.org/10.1063/1.3531996
[34] G. Marius, *The Physics of Semiconductors: Kramers-kronig Relations*, (Springer, Berlin Heidelberg, 2010). pp. 775–776. ISBN-13 978-3-540-25370-9
[35] M. Gajdoš, K. Hummer, G. Kresse, J. Furthmüller, and F. Bechstedt, Linear optical properties in the projector-augmented wave methodology. Phys. Rev. B, **73**, 045112 (2006). https://doi.org/10.1103/PhysRevB.73.045112
[36] C. Ambrosch-Draxl, J.O. Sofo, Linear optical properties of solids within the full potential linearized augmented planewave method. Comput. Phys. Commun **175**, 1 (2006). https://doi.org/10.1016/j.cpc.2006.03.005
[37] M. Irfan, M.A. Kamran, S. Azam, M.W. Iqbal, T. Alharbi, A. Majid, S.B. Omran, R. Khenata, A. Bouhemadou, and X. Wang, Electronic structure and optical properties of TaNO: an ab initio study, J. Mol. Graph. Model. **92**, 296 (2019). https://doi.org/10.1016/j.jmgm.2019.08.006
[38] D.R. Penn, Wave-Number-Dependent Dielectric Function of Semiconductors, Phys. Rev. **128**, 2093 (1962). https://doi.org/10.1103/PhysRev.128.2093
[39] A. Benzina, First-principles calculation of structural, optoelectronic properties of the cubic $Al_xGa_yIn_{1-x-y}N$ quaternary alloys matching on AlN substrate, within modified Becke-Johnson (mBJ) exchange potential, Optik, **127**, 11577 (2016). https://doi.org/10.1016/j.ijleo.2016.09.014
[40] S. Samanta, and S.M. Saini, First-principle calculations of electronic and optical properties of $CdCr_2Te_4$ spinel: use of mBJ + U potential in narrow band gap semiconductors, Indian J. Phys. **93**(3), 335 (2019). https://doi.org/10.1007/s12648-018-1298-x
[41] N. Yaqoob, et al, Structural, electronic, magnetic, optical and thermoelectric response of half-metallic $AMnTe_2$ (A = Li, Na, K): An ab-initio calculations, Physica B: Condensed Matter, **574**, 311656 (2019). https://doi.org/10.1016/j.physb.2019.08.033
[42] D. Vasileska, H.R. Khan, S.S. Ahmed, C. Ringhofer, and C. Heitzinger, Quantum and Coulomb Effects in Nano Devices, International Journal of Nanoscience, **4**, 305 (2005). https://doi.org/10.1142/S0219581X05003164
[43] A. Reshak, Thermoelectric properties of the spin-polarized half-metallic ferromagnetic CsTe and RbSe compounds, RSC Adv. **6**, 98197 (2016). https://doi.org/10.1039/C6RA22758A
[44] V.F. Gantmakher, The experimental study of electron-phonon scattering in metals, Reports on progress in physics, **37**(3), 317 (1974). https://doi.org/10.1088/0034-4885/37/3/001
[45] C. Lee et al., Density functional theory investigation of the electronic structure and thermoelectric properties of layered MoS_2, $MoSe_2$ and their mixed-layer compound, J. Solid State Chem. **211**, 113 (2014). https://doi.org/10.1016/j.jssc.2013.12.012
[46] T.M. Tritt, Thermoelectric phenomena, materials, and applications, Annu. Rev. Mater. Res. **41**, 433 (2011). https://doi.org/10.1146/annurev-matsci-062910-100453
[47] A. Besbes et al. First-principles study of structural, electronic, thermodynamic, and thermoelectric properties of a new ternary half-Heusler alloy PdZrGe, Chinese Journal of Physics, **56**, 2926 (2018). https://doi.org/10.1016/j.cjph.2018.09.027

[48] S.Yousuf, D.C. Gupta, Unravelling the magnetism, high spin polarization and thermoelectric efficiency of ZrFeSi half-Heusler, physica B: condensed matter, **534**, 5 (2018). https://doi.org/10.1016/j.physb.2018.01.011
[49] S. Parsamehr et al., Half-Metallic, Thermoelectric, Optical, and Thermodynamic Phase Stability of RbBaB (001) Film: A DFT Study, International Journal of Thermophysics, **40**, 64 (2019). https://doi.org/10.1007/s10765-019-2531-3
[50] S. Singh, and D.C. Gupta, Investigation of Electronic, Magnetic, Thermodynamic, and Thermoelectric Properties of Half-Metallic XLiSn (X = Ce, Nd) Alloys, Journal of Superconductivity and Novel Magnetism, **32**, 2009 (2019). https://doi.org/10.1007/s10948-018-4907-1
[51] A. Besbes et al., Optical and thermoelectric response of RhTiSb half-Heusler, International Journal of Modern Physics B, **33**(22) 1950247 (2019). https://doi.org/10.1142/S0217979219502473

ОГЛЯД ЕЛЕКТРОННИХ ОПТИЧНІ ТА ТРАНСПОРТНИХ ВЛАСТИВОСТЕЙ НАПІВГЕЙСЛЕРОВОГО СПЛАВУ: NiVSi

Джелті Радуан[a], Бесбес Анісса, Бестані Бенауда[b]
[a]Лабораторія технологій та властивостей твердих речовин, Університет Мостаганем (UMAB) – Алжир
[b]Лабораторія EA2M, Університет Мостаганем (UMAB) – Алжир

Теоретично досліджено напівгейслеровий сплав NiVSi за допомогою розрахунків за першопринципами на основі теорії функціоналу щільності (DFT). Для кращого опису електронних властивостей обмінно-кореляційного потенціалу використовується потенціал TB-mBJ. Структурні, електронні, магнітні, оптичні та термоелектричні властивості були розраховані за допомогою програмного забезпечення WIEN2k. Знайдені негативні енергії когезії та енергії формування показують, що NiVSi є термодинамічно стабільним. З електронної точки зору NiVSi є напівметалом з непрямою забороненою зоною 0,73 еВ у каналі зі спіном вниз, тоді як канал зі спіном вгору є металевим. Загальний магнітний момент дорівнює 1. Оптично, отриманий високий коефіцієнт поглинання в ультрафіолетовому діапазоні довжин хвиль робить NiVSi корисним як ефективний поглинач ультрафіолетового випромінювання. Термоелектрично було отримано високу якість в області p- і n-типу, що робить цю сполуку функціональною для термоелектричних застосувань. Генерація повністю спін-поляризованого струму робить цю сполуку непридатною для застосування спінтронів при кімнатній температурі, легування може бути задовільним рішенням для покращення цієї властивості.

Ключові слова: DFT; підхід mBJ; напівметалевий; ультрафіолетовий; фактор якості.